Hindawi Publishing Corporation
Journal of Control Science and Engineering
Volume 2015, Article ID 680809, 16 pages
http://dx.doi.org/10.1155/2015/680809

Research Article

High-Order Sliding Mode-Based Synchronous Control of a Novel Stair-Climbing Wheelchair Robot

Juanxiu Liu, Yifei Wu, Jian Guo, and Qingwei Chen

School of Automation, Nanjing University of Science and Technology, Nanjing 210094, China

Correspondence should be addressed to Yifei Wu; wuyifei0911@163.com

Received 27 April 2015; Revised 3 September 2015; Accepted 9 September 2015

Academic Editor: Hung-Yuan Chung

For the attitude control of a novel stair-climbing wheelchair with inertial uncertainties and external disturbance torques, a new synchronous control method is proposed via combing high-order sliding mode control techniques with cross-coupling techniques. For this purpose, a proper controller is designed, which can improve the performance of the system under conditions of uncertainties and torque perturbations and also can guarantee the synchronization of the system. Firstly, a robust high-order sliding mode control law is designed to track the desired position trajectories effectively. Secondly, considering the coordination of the multiple joints, a high-order sliding mode synchronization controller is designed to reduce the synchronization errors and tracking errors based on the controller designed previously. Stability of the closed-loop system is proved by Lyapunov theory. The simulation is performed by MATLAB to verify the effectiveness of the proposed controller. By comparing the simulation results of two controllers, it is obvious that the proposed scheme has better performance and stronger robustness.

1. Introduction

With the rapid increase of the elderly population over the age of 60, population aging will be an outstanding performance of global population trends in the 21st century. Aging society brings a lot of problems, such as nursing for the elderly and medical problems. At the same time, thousands of people lost the ability to walk each year caused by a variety of accidents, natural disasters, and diseases. With the development of the society and the improvement of human civilization, the people with disabilities need to use modern high-tech to improve their freedom and quality of life. Hence, wheelchair robot used to help the disabled or elderly people walking has become a hot research area in recent years.

Although the barrier-free accessibility has been disseminated in recent years, stairs and other architectural barriers still exist in many cities and buildings. Since the standard wheelchair has no capability of crossing barriers, a number of stair-climbing wheelchairs which can help the disabled or elderly people overcoming obstacles have been researched. The common stair-climbing mechanisms used in the stair-climbing wheelchairs are tracks, wheels, and hybrid structures. Tracked stair-climbing wheelchair can guarantee the stability of the users in the process of ascending and descending stairs. Lawn et al. [1] designed a tracked wheelchair capable of negotiating large number of twisting and irregular stairs. In [2], a wheelchair using cluster wheels was developed. The wheelchair seat was kept stable during the stairs ascending process and the user needed not to face down the stairs. In [3], Wheelchair.q using triple cluster wheels was designed. The cluster wheels systems usually have complex mechanisms and the stability is lower than crawler systems. A stair-climbing robot with legs and wheels was designed in [4]. Chen and Pham [5] designed a prototype which was comprised of a pair of rotational multilimbed structures. There are some other design schemes adopting hybrid structures in [6–8].

Since the stair-climbing wheelchair is used in complex terrain, the first thing that should be considered is high precious position control for wheelchair system. In [2], PID control was used to provide appropriate torque during climbing process. A fuzzy controller was applied to correct the errors in direction and position misalignment, so that the final posture of the tracked mobile robot was corrected in [9]. In [10], an active tension control law combined with the computed torque method was obtained for wheelchair

robot during the stair-climbing process, which can track the reference input curve of homonymic constraint force when tracking reference input curve of each joint. Although the control strategies mentioned above can make some efforts for the control of stair-climbing wheelchair, various system uncertainties and torque perturbations were not taken into consideration.

Since the sliding mode control has strong robustness for system disturbances and unmodeled dynamics, it has been widely used in robot control. Conventional sliding mode control can achieve the first-order sliding motion of the system states, which means the relative degree of the sliding variable s is 1. When the system states slide along the preset manifold, only the sliding variable is guaranteed to converge to zero, and its derivative is nonsmooth, so the chattering phenomenon always comes up in the sliding mode control system. In order to solve the chattering which exists in conventional sliding mode control, a variety of methods were proposed such as state-dependent gain method, observer-based chattering suppression, and the high-order sliding model control (HOSMC) in [11, 12]. In [13], with the HOSMC used in attitude control of large-scale spacecraft, the robustness of the system with respect to uncertainties and external disturbances was improved, and the chattering phenomenon was attenuated. In [14], a HOSMC was designed for a flexible link space robotic arm with payload, which exploited the robustness properties of SMC, while also increasing accuracy by reducing chattering effects.

Another important problem that should be considered is the coordination of the stair-climbing wheelchair system due to its characteristic of multiple joints. If the stair-climbing wheelchair works in a noncoordination manner, the assembly task will be failed, and a more serious consequence is that the users will be injured. In [15], a new control approach to position synchronization of multiple motion axes was developed, by incorporating cross-coupling technology into adaptive control architecture. A novel robust adaptive terminal sliding mode position synchronized control approach was proposed for the operation of multiple motion axes system and the convergence of position errors and synchronization errors could be guaranteed in [16]. In [17], the synchronous control of a dual linear motor servosystem was developed by a cross-coupled intelligent complementary sliding mode control system; a better control performance and robustness with regard to uncertainties can be achieved.

The motivation of the presented work here is to find a proper controller which has strong rejection capacity against external disturbances and robustness to deal with uncertainties and also can guarantee the synchronization of the system. Based on a novel stair-climbing wheelchair robot which was designed in [18], a new control method is proposed in this paper via combining the HOSMC techniques and cross-coupling techniques. The mechanical structure of the stair-climbing robot is described at first, and then its dynamics with uncertainties and perturbations is analyzed. After that, single joint position tracking controller adopting HOSMC techniques is designed to assure the high accuracy tracking under conditions of uncertainties and torque perturbations, and then a synchronous controller based on HOSMC techniques and cross-coupling techniques is developed to reduce the synchronization errors and position errors at the same time. The stability of the closed-loop system is proved by Lyapunov theory. In the last section, simulations are completed under the same condition by using the HOSM controller and the HOSM synchronous controller, respectively. The two results are compared to validate the effectiveness of the proposed method.

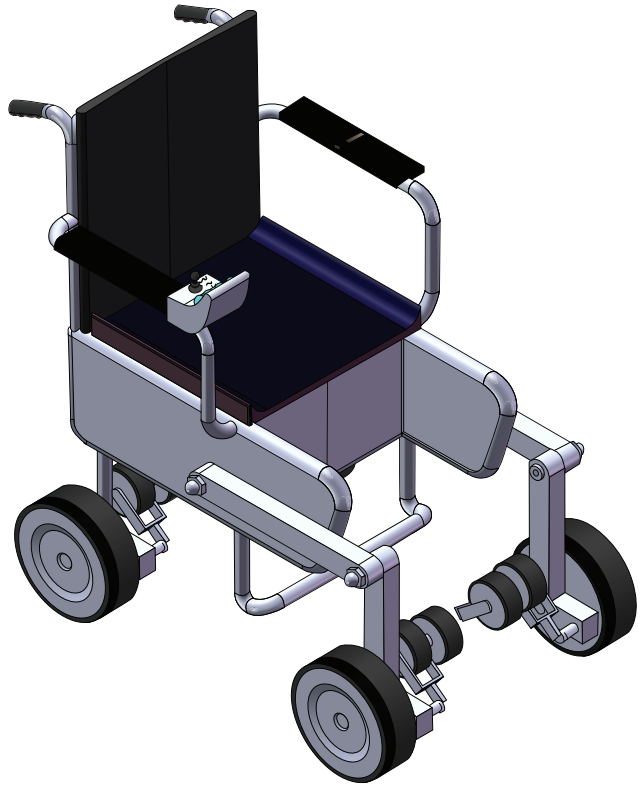

Figure 1: Virtual prototype of wheelchair.

This paper is organized as follows. Section 2 describes mechanical structure of the stair-climbing wheelchair and its dynamic model with uncertainties and perturbations. In Section 3, a HOSM position controller and a HOSM synchronous controller are proposed and the stability of the closed-loop system is analyzed. Section 4 presents the simulation results. Finally, the conclusion is given in Section 5.

2. System Description and Modeling

2.1. System Description. It seems to be a quite complex problem to design a staircase climbing wheelchair which is adaptable to various terrains. However, this problem can be solved by simply splitting the process of staircase climbing into two different problems: (a) climbing a single step of variable height; (b) providing stability for the entire mechanism while the wheelchair is on the stair [19]. Based on this design idea, a stair-climbing wheelchair is proposed. Figure 1 shows the virtual prototype of the stair-climbing wheelchair. Figure 2 presents the structure of one side of the wheelchair. The parts of climbing mechanism and two-link

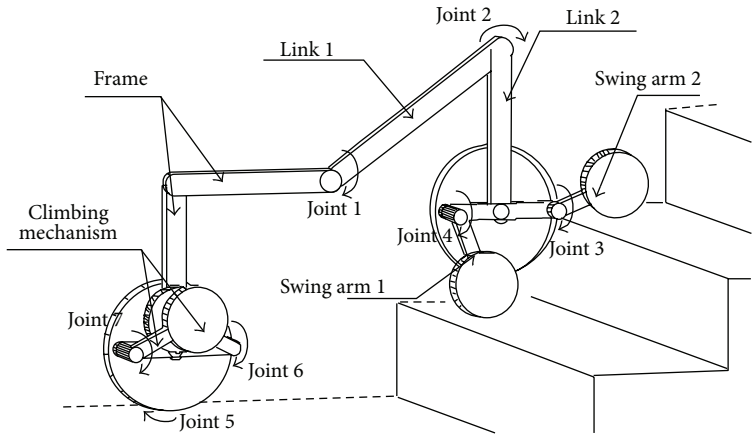

Figure 2: Mechanical structure of wheelchair.

mechanism are shown in Figure 2. In this system, all joints are revolute joints driven by motors. The climbing mechanisms, the wheels, and the two-link mechanisms are independent of each other.

The climbing mechanism which contains two swing arms (Figure 2) is designed to surmount a single step. The system has four such climbing mechanisms: two front and two rear. The front climbing mechanisms are joined to two-link mechanism, and the rear mechanisms are fixed on the frame. When the wheelchair reaches a step, the swing arms which are driven by motors rotate at a constant speed. When the swing arms touch the top of the step, the wheelchair's weight is supported by them. The front wheels can now be lifted to surmount the step. When the front wheels touch the top of the step, the weight is now transferred to them. The swing arms continue to rotate to their original positions. This process ends, and the system is now ready to climb the next step.

The two-link mechanism is designed to ensure the wheelchair seat always stays at the upright position. Because the wheelchair seat is joined to the frame, when the front wheels rise, the frame will rotate. This should be adjusted by link mechanism. Similarly, the rear climbing mechanisms move when the top of staircase is reached, and the link mechanism should accommodate the seat.

The task of the sensorial system is to measure the distances between the wheels and the steps and the information about the steps. Proposed placement of stair sensors is shown in Figure 3. Two ultrasound sensors are placed on front wheels in horizontal position to detect stair edge. To measure the distances to next step, two ultrasound sensors are placed on the link mechanism in horizontal position. The width of the step can be calculated by comparing the data of two sets of sensors. There are fourteen rotary transformers (one per joint) to ensure each joint position is measurable. When the positions of the joints are known, the height of swing arms relative to the ground can be calculated, which is defined as h_1. Then, two ultrasound sensors are placed on front climbing mechanisms in vertical position to measure the height of swing arms relative to the step, which can be defined as h_2. So the step height is the height difference between h_1 and h_2. Finally, two ultrasound sensors are placed on the frame to measure the positions of rear wheels with respect to the stair edge.

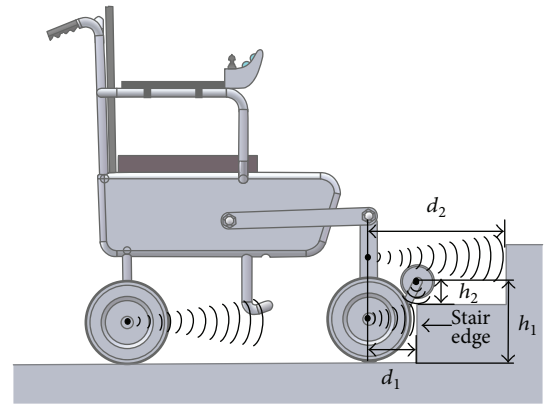

Figure 3: Proposed stair sensor placement.

The process of climbing stairs is shown in Figure 4 and achieved by the following steps.

(1) When the front wheels sense a step, the front climbing mechanisms rotate up at a speed defined by the program. At the same time, the two-link mechanisms also rotate for adjusting the attitude of the seat. The front wheels are raised to surmount the step. The wheelchair moves forward until next step is sensed.

(2) Repeat step (1) until the wheelchair surmounts the second step.

(3) The front and rear climbing mechanisms climb synchronously.

(4) When the top of the staircase is reached, the front climbing mechanisms detect no step edge and remain motionless. The rear mechanisms continue to move to the top of the stair.

2.2. System Kinematics and Dynamics. In order to analyze the model of wheelchair, some assumptions are made as follows.

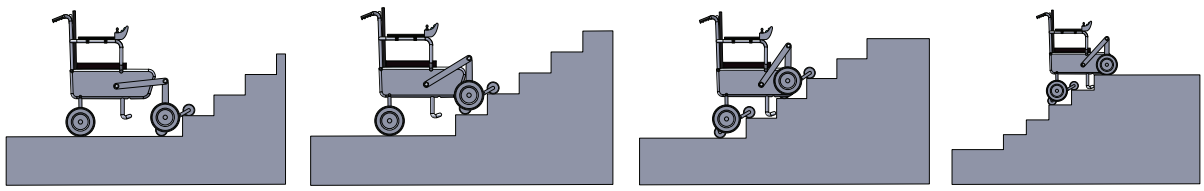

Figure 4: Steps of stairs ascending process.

Assumption 1. The wheelchair is a rigid body system. The tires are point contact with the ground, and the contact points have no relative sliding. The tires have no elastic deformation.

Assumption 2. The structure of the robot is symmetrical, so the dynamic analysis is based on the structure which is simplified to planar mechanism.

Assumption 3. The position and attitude of wheelchair are not affected by active control. Each joint has one rotational degree-of-freedom, and the joints are affected by active control.

Figure 5 shows the kinematic scheme of stair-climbing wheelchair. l_i $(i = 1, 2, \ldots, 7)$ is the length of wheelchair's each part. R is the radius of wheels, and r is the radius of small wheels. h is the step height. d is the width of the step. d_1 is the distance between the front wheels and the step edge. q_i $(i = 1, 2, \ldots, 7)$ is the angle of joint i. δ is the original angle of the swing arm. q_0, $\dot{q}_0$, and $\ddot{q}_0$ denote the angle of the seat with respect to ground, velocity, and acceleration, respectively. p_g is the wheelchair's center of gravity. m_i and j_i are the mass and moment of inertia of wheelchair's each part, respectively.

The desired trajectories can be determined by the inverse kinematic model according to the kinematic parameters above. Define the q_{di} $(i = 0, 1, \ldots, 7)$ as desired trajectory of the joint i. For the safety of user, the trajectories must satisfy $q_{d0} = \dot{q}_{d0} = \ddot{q}_{d0} = 0$, making sure that the wheelchair seat always stays at the upright position. For simplicity, the inverse kinematic model is given here, and the derivation process is presented in [20]. When the wheelchair climbs the first and second steps, the inverse kinematic model is the following:

$$
\begin{aligned}
q_{d0} &= 0,\\
q_{d1} &= \arcsin\left[\frac{(h + r + l_4 + l_6\sin(-\delta - q_{d3}) - R - l_1 - l_2\sin(q_{d0}))}{l_3}\right],\\
q_{d2} &= \frac{\pi}{2} - q_{d1},\\
q_{d3} &= -\delta + vt,\\
q_{d4} &= -\pi + \delta + vt,\\
q_{d5} &= \frac{[d + R - d_1 + l_1\sin(q_{d0}) + l_2(1 - \cos(q_{d0})) + l_3(1 - \cos(q_{d0} + q_{d1}))]}{l_3},\\
q_{d6} &= -\delta,\\
q_{d7} &= -\pi + \delta,
\end{aligned}
\tag{1}
$$

where v is the set rotational speed of climbing mechanisms. When h, d, and d_1 are accurately measured by sensorial system, the desired trajectories can be generated by (1).

According to the previous works in [20], the dynamics can be well approximated by the following equation:

$$M(q)\ddot{q} + C(q, \dot{q})\dot{q} + G(q) = \tau, \tag{2}$$

where q is a vector of generalized coordinates, $q = [q_0, q_1, \ldots, q_n]^T \in R^8$, and $\dot{q}$ and $\ddot{q}$ are velocity vector and acceleration vector, respectively. $M(q) \in R^{8\times 8}$ is the positive definite symmetric inertial matrix. $C(q, \dot{q}) \in R^{8\times 8}$ is the matrix containing Coriolis force and centripetal force. $G(q) \in R^8$ is the gravity vector and $\tau = [\tau_0, \tau_1, \ldots, \tau_7] \in R^8$ is torque input vector. The detailed expressions can be found in the Appendix.

In practical applications, there are a lot of uncertain factors such as friction and disturbing torque. Considering the uncertainties and the modeling errors, the dynamic equation (2) can be rewritten as follows:

$$M_0(q)\ddot{q} + C_0(q, \dot{q})\dot{q} + G_0(q) = \tau + \rho(t), \tag{3}$$

$$\rho(t) = d(t) - \Delta M(q)\ddot{q} - \Delta C(q, \dot{q})\dot{q} - \Delta G(q), \tag{4}$$

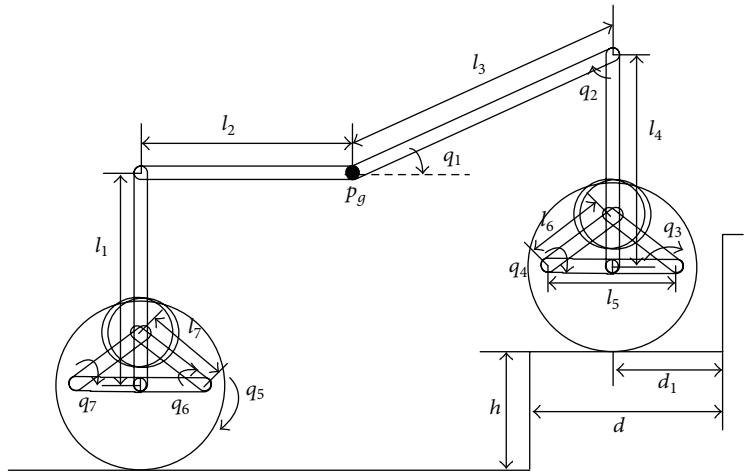

Figure 5: Kinematic scheme of stair-climbing wheelchair.

where $M_0(q)$, $C_0(q,\dot{q})$, and $G_0(q)$ are nominal values of $M(q)$, $C(q,\dot{q})$, and $G(q)$, respectively. $\Delta M(q)$, $\Delta C(q,\dot{q})$, and $\Delta G(q)$ are uncertainties of $M(q)$, $C(q,\dot{q})$, and $G(q)$, respectively. $d(t)$ is torque perturbations vector, and $\rho(t) \in R^8$ denotes the total uncertainties of the dynamics caused by parameter variations and perturbations.

Some assumptions for the system parameters and variables are made as follows.

Assumption 4. $M_0(q)$ is a positively definite matrix, and there are known positive constants $M_{\max}$ and $M'_{\max}$ such that the following inequalities hold: $\|{M_0}^{-1}(q)\| \leq M_{\max}$ and $\|\dot{M}_0^{-1}(q)\| \leq M'_{\max}$.

Assumption 5. There are known positive constants $\rho_{\max}$ and $\rho'_{\max}$ satisfying the following inequalities: $\|\rho(t)\| \leq \rho_{\max}$ and $\|\dot{\rho}(t)\| \leq \rho'_{\max}$.

3. Control System Design and Stability Analysis

The wheelchair kinematics and dynamics have been given in the previous section, which may make the controller design complicated. A robust control law with respect to uncertainties and perturbations is needed in the high accuracy position tracking of the stair-climbing wheelchair system. In this paper, single joint position tracking controller and a synchronous controller are developed, respectively. Stability of the closed-loop system is analyzed by Lyapunov theory. Here is the design process in detail.

3.1. HOSM Controller Design. This section considers the position tracking problem for wheelchair joints, the kinematic and dynamic parameters are known, and the desired trajectory is denoted as q_{di}. The measureable states are joint position q_i and the joint velocity $\dot{q}_i$. The control objective is to design robust chattering-free control signal τ, which ensures that q_i always tracks the desired trajectory q_{di}, in spite of the inertial uncertainties and external disturbance torques.

The position tracking error of a single joint is defined as

$$e_i = q_i - q_{di}. \tag{5}$$

Set $s = [e_1, e_2, \ldots, e_n]^T \in R^n$, in order to achieve HOSM control of sliding variable s, we define σ as

$$\sigma = \ddot{s} + c_1\dot{s} + c_0 s, \tag{6}$$

where c_1 and c_0 are both positive constants. The HOSM control law for sliding variable s is as follows:

$$\tau = u_{eq} + M_0(q)\, u_{vss}, \tag{7}$$

$$\begin{aligned} u_{eq} = {} & M_0(q)\,\ddot{q}_d + C_0(q,\dot{q})\,\dot{q} + G_0(q) \\ & + M_0(q)\,(-c_1\dot{s} - c_0 s), \end{aligned} \tag{8}$$

$$\dot{u}_{vss} = -k_1\sigma - k_2\frac{\sigma}{\|\sigma\|}, \tag{9}$$

where k_1 and k_2 are positive constants, satisfying $k_1 > 0$ and $k_2 > \|\dot{M}_0^{-1}(q)\|\|\rho(t)\| + \|{M_0}^{-1}(q)\|\|\dot{\rho}(t)\|$.

Theorem 1. *Considering system (3), the sliding surface defined in (6) is chosen. When the parameters satisfy $k_1 > 0$ and $k_2 > \|\dot{M}_0^{-1}(q)\|\|\rho(t)\| + \|{M_0}^{-1}(q)\|\|\dot{\rho}(t)\|$, the position tracking error fulfills the condition that $\lim_{t\to\infty} s = 0$, under the control effort of the control law given in (7).*

Proof. Choose the following Lyapunov function:

$$V = \frac{1}{2}\sigma^T\sigma. \tag{10}$$

Taking the time derivative of V, it can be written as

$$\dot{V} = \sigma^T\dot{\sigma} = \sigma^T\left(\dddot{s} + c_1\ddot{s} + c_0\dot{s}\right). \tag{11}$$

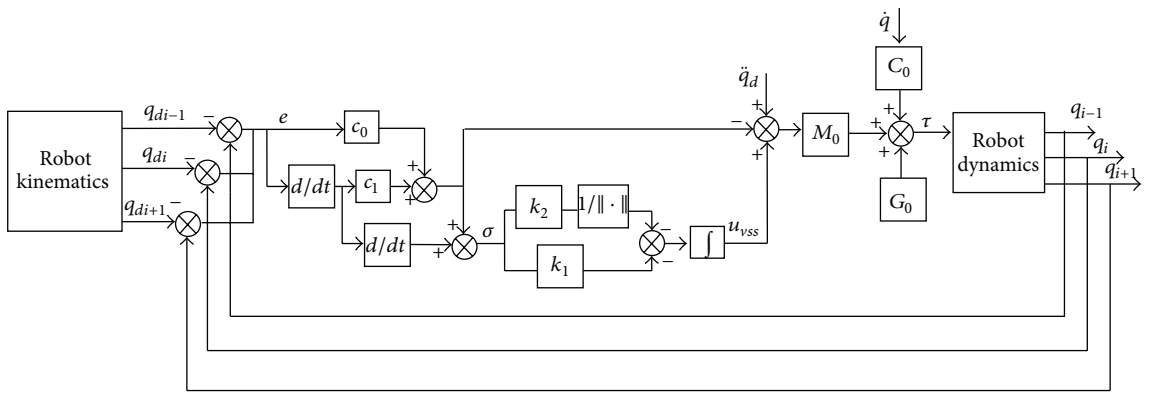

Figure 6: Structure of the HOSM controller.

Differentiating (5) and taking (3) yield

$$\begin{aligned}\ddot{s} &= \ddot{q} - \ddot{q}_d \\ &= M_0^{-1}(q)\left(\tau + \rho(t) - G_0(q) - C_0(q,\dot{q})\dot{q}\right) - \ddot{q}_d.\end{aligned} \tag{12}$$

Substituting (7), (8), and (9) into (12), we have

$$\begin{aligned}\ddot{s} &= M_0^{-1}(q)\left[M_0(q)\ddot{q}_d + \rho(t) + M_0(q)\left(-c_1\dot{s} - c_0 s\right)\right. \\ &\quad \left. + M_0(q)u_{vss}\right] - \ddot{q}_d = M_0^{-1}(q)\rho(t) - c_1\dot{s} - c_0 s \\ &\quad + u_{vss}.\end{aligned} \tag{13}$$

Differentiating (13), and considering (9), it can be obtained as follows:

$$\begin{aligned}\dddot{s} &= \dot{M}_0^{-1}(q)\rho(t) + M_0^{-1}(q)\dot{\rho}(t) - c_1\ddot{s} - c_0\dot{s} + \dot{u}_{vss} \\ &= \dot{M}_0^{-1}(q)\rho(t) + M_0^{-1}(q)\dot{\rho}(t) - c_1\ddot{s} - c_0\dot{s} - k_1\sigma \\ &\quad - k_2\frac{\sigma}{\|\sigma\|}.\end{aligned} \tag{14}$$

Substituting (14) into (11), we get

$$\begin{aligned}\dot{V} &= \sigma^T\left(\dot{M}_0^{-1}(q)\rho(t) + M_0^{-1}(q)\dot{\rho}(t) - c_1\ddot{s} - c_0\dot{s}\right. \\ &\quad \left. - k_1\sigma - k_2\frac{\sigma}{\|\sigma\|} + c_1\ddot{s} + c_0\dot{s}\right) = \sigma^T\dot{M}_0^{-1}(q)\rho(t) \\ &\quad + \sigma^T M_0^{-1}(q)\dot{\rho}(t) - \sigma^T k_1\sigma - k_2\|\sigma\| \le \left\|\sigma^T\right\| \\ &\quad \cdot \left\|\dot{M}_0^{-1}(q)\right\|\|\rho(t)\| + \left\|\sigma^T\right\|\left\|M_0^{-1}(q)\right\|\|\dot{\rho}(t)\| \\ &\quad - \sigma^T k_1\sigma - k_2\|\sigma\| = \left\|\sigma^T\right\|\left(\left\|\dot{M}_0^{-1}(q)\right\|\|\rho(t)\|\right. \\ &\quad \left. + \left\|M_0^{-1}(q)\right\|\|\dot{\rho}(t)\| - k_2\right) - \sigma^T k_1\sigma < -\sigma^T k_1\sigma.\end{aligned} \tag{15}$$

Therefore, $\sigma^T\dot{\sigma} < 0$, when $\|\sigma\| \neq 0$, the system is asymptotically stable, and $\lim_{t\to\infty} s = 0$ also can be assured. □

From Theorem 1, it can be obtained that the tracking error can converge to zero in spite of uncertainties and perturbation. Figure 6 presents the structure of the HOSM position tracking controller without coordinating the motion of each joint. With the information provided by sensorial system, the reference trajectory q_{di} is obtained by using the inverse kinematic model. The tracking error e_i can be obtained by the feedback signal, and then the controller calculates the joint driving moment τ which is applied to the dynamic model for joint control.

3.2. HOSM Synchronous Controller Design. Because the position and attitude of the wheelchair are affected by each joint's motion, the coordination among the joints is needed to be considered besides the position tracking error of each joint. If the motions of climbing mechanisms are asynchronous, the seat will lean in the process of climbing stairs, and it will result in a series of problems such as the system damage and injury accidents. This section considers the synchronization problem of multiple joints system. The control objective is to design robust chattering-free control signal τ', which ensures that the position tracking error and synchronization error converge to zero, when q_{di}, q_i, and $\dot{q}_i$ are known.

For a multiple joints system, the position tracking errors must satisfy the following condition in [15]:

$$\lim_{t\to\infty} e_1 = \lim_{t\to\infty} e_2 = \cdots = \lim_{t\to\infty} e_n = 0. \tag{16}$$

Considering (17), the synchronization errors are defined as

$$\begin{aligned}\varepsilon_1 &= e_1 - e_2 + e_1, \\ \varepsilon_2 &= e_2 - e_3 + e_2 - e_1, \\ &\vdots \\ \varepsilon_i &= e_i - e_{i+1} + e_i - e_{i-1}, \\ &\vdots \\ \varepsilon_n &= e_n + e_n - e_{n-1}.\end{aligned} \tag{17}$$

The expression means that the synchronization errors of the multiple joints system ε_i are defined as differential position errors among multiple joints system. Setting $\varepsilon = [\varepsilon_1, \varepsilon_2, \ldots, \varepsilon_n]^T \in R^n$, function (17) can be written as

$$\begin{bmatrix} \varepsilon_1 \\ \varepsilon_2 \\ \vdots \\ \varepsilon_{n-1} \\ \varepsilon_n \end{bmatrix} = \begin{bmatrix} 2 & -1 & 0 & \cdots & 0 \\ -1 & 2 & -1 & \cdots & 0 \\ \vdots & \ddots & \ddots & \ddots & \vdots \\ 0 & \cdots & -1 & 2 & -1 \\ 0 & 0 & \cdots & -1 & 2 \end{bmatrix} \begin{bmatrix} e_1 \\ e_2 \\ \vdots \\ e_{n-1} \\ e_n \end{bmatrix} = Te, \tag{18}$$

where T is the positive definite matrix.

Setting $s_2 = \varepsilon$, in order to achieve HOSM control of sliding variable s_2, define σ_s as

$$\sigma_s = \ddot{s}_2 + c_1 \dot{s}_2 + c_0 s_2. \tag{19}$$

Substituting (18), there is

$$\sigma_s = T\ddot{s} + c_1 T\dot{s} + c_0 Ts. \tag{20}$$

The HOSM control law for sliding variable s_2 is designed as

$$\dot{u}'_{vss} = -k_3\sigma_s - k_4 \frac{\sigma_s}{\|\sigma_s\|}, \tag{21}$$

where $k_3 > 0$ and $k_4 > \|\dot{M}_0{}^{-1}(q)\|\|\rho(t)\| + \|M_0{}^{-1}(q)\|\|\dot{\rho}(t)\|$.

The HOSM synchronous control law which is the overall control law is developed as follows:

$$\tau' = u_{eq} + M_0(q)\, u_{vss} + M_0(q)\, u'_{vss}. \tag{22}$$

Theorem 2. *Considering system (3), the sliding surface defined in (19) is chosen. When the parameters satisfy $k_1 > 0$, $k_2 > \|\dot{M}_0{}^{-1}(q)\|\|\rho(t)\| + \|M_0{}^{-1}(q)\|\|\dot{\rho}(t)\|$, $k_4 > \|\dot{M}_0{}^{-1}(q)\|\|\rho(t)\| + \|M_0{}^{-1}(q)\|\|\dot{\rho}(t)\|$, and $k_3 > 0$, the position tracking error e and synchronization error ε can converge to zero simultaneously, under the control effort of the control law given in (22).*

Proof. Choose the following Lyapunov function:

$$V = \frac{1}{2}\sigma^T\sigma + \frac{1}{2}\sigma_s^T T^{-1}\sigma_s. \tag{23}$$

Differentiating V with respect to time yields

$$\dot{V} = \sigma^T\dot{\sigma} + \sigma_s^T T^{-1}\dot{\sigma}_s. \tag{24}$$

Considering (14), and differentiating (6) and (20), we get

$$\begin{aligned} \dot{\sigma} &= \dot{u}_{vss} + \dot{u}'_{vss} + \dot{M}_0{}^{-1}(q)\,\rho(t) + M_0{}^{-1}(q)\,\dot{\rho}(t), \\ \dot{\sigma}_s &= T\dot{u}_{vss} + T\dot{u}'_{vss} + T\dot{M}_0{}^{-1}(q)\,\rho(t) \\ &\quad + TM_0{}^{-1}(q)\,\dot{\rho}(t). \end{aligned} \tag{25}$$

Substituting (25) into (24), we have

$$\begin{aligned} \sigma^T\dot{\sigma} &= \sigma^T\Bigg(\dot{M}_0{}^{-1}(q)\,\rho(t) + M_0{}^{-1}(q)\,\dot{\rho}(t) - k_1\sigma \\ &\quad - k_2\frac{\sigma}{\|\sigma\|} - k_3\sigma_s - k_4\frac{\sigma_s}{\|\sigma_s\|}\Bigg) = \sigma^T\dot{M}_0{}^{-1}(q)\,\rho(t) \\ &\quad + \sigma^T M_0{}^{-1}(q)\,\dot{\rho}(t) - \sigma^T k_1\sigma - k_2\|\sigma\| - \sigma^T k_3\sigma_s \\ &\quad - \sigma^T k_4\frac{\sigma_s}{\|\sigma_s\|} \le \left\|\sigma^T\right\|\left\|\dot{M}_0{}^{-1}(q)\right\|\|\rho(t)\| + \left\|\sigma^T\right\| \\ &\quad \cdot \left\|M_0{}^{-1}(q)\right\|\|\dot{\rho}(t)\| - \sigma^T k_1\sigma - k_2\|\sigma\| - \sigma^T k_3 T\sigma \\ &\quad - k_4\frac{\sigma^T T\sigma}{\|\sigma_s\|} = \left\|\sigma^T\right\|\left(\left\|\dot{M}_0{}^{-1}(q)\right\|\|\rho(t)\|\right. \\ &\quad \left. + \left\|M_0{}^{-1}(q)\right\|\|\dot{\rho}(t)\| - k_2\right) - \sigma^T k_1\sigma - \sigma^T k_3 T\sigma \\ &\quad - k_4\frac{\sigma^T T\sigma}{\|\sigma_s\|} < -\sigma^T k_1\sigma - \sigma^T k_3 T\sigma - k_4\frac{\sigma^T T\sigma}{\|\sigma_s\|}, \end{aligned} \tag{26}$$

$$\begin{aligned} \sigma_s^T T^{-1}\dot{\sigma}_s &= \sigma_s^T T^{-1} T\Bigg(\dot{M}_0{}^{-1}(q)\,\rho(t) + M_0{}^{-1}(q)\,\dot{\rho}(t) \\ &\quad - k_1\sigma - k_2\frac{\sigma}{\|\sigma\|} - k_3\sigma_s - k_4\frac{\sigma_s}{\|\sigma_s\|}\Bigg) = \sigma_s^T\dot{M}_0{}^{-1}(q) \\ &\quad \cdot \rho(t) + \sigma_s^T M_0{}^{-1}(q)\,\dot{\rho}(t) - \sigma^T T k_1\sigma - \frac{\sigma^T T k_2\sigma}{\|\sigma\|} \\ &\quad - \sigma_s^T k_3\sigma_s - k_4\sigma_s \le \left\|\sigma_s^T\right\|\left(\left\|\dot{M}_0{}^{-1}(q)\right\|\|\rho(t)\|\right. \\ &\quad \left. + \left\|M_0{}^{-1}(q)\right\|\|\dot{\rho}(t)\| - k_4\right) - \sigma^T T k_1\sigma - \frac{\sigma^T T k_2\sigma}{\|\sigma\|} \\ &\quad - \sigma_s^T k_3\sigma_s < -\sigma^T T k_1\sigma - \frac{\sigma^T T k_2\sigma}{\|\sigma\|} - \sigma_s^T k_3\sigma_s. \end{aligned}$$

□

From (18), T is positive definite matrix, so it can be obtained that $\sigma^T\dot{\sigma} < 0$ and $\sigma_s^T T^{-1}\dot{\sigma}_s < 0$. It is proved that the system is stable simultaneously, and the convergence of the position tracking error e and synchronization error ε is assured; that is, $\lim_{t\to\infty} s = 0$ and $\lim_{t\to\infty}\varepsilon = 0$. Figure 7 presents the structure of the HOSM synchronous controller. It can be found that the synchronous control signal is added to the HOSMC control signal.

4. Simulation Results

To demonstrate the performance of the proposed approach in Section 3, simulations are performed by MATLAB. In this section, the HOSM controller and HOSM synchronous

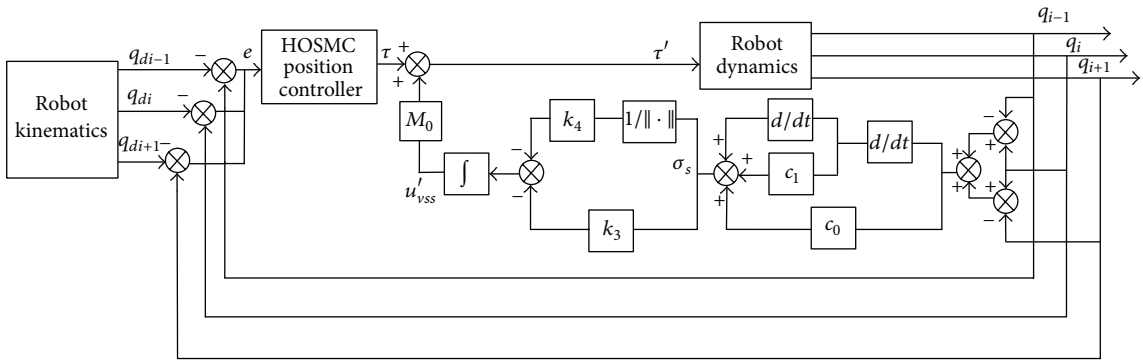

Figure 7: Structure of the HOSM synchronous controller.

controller are used to control the dynamic model of the wheelchair, respectively.

The values of kinematic and dynamic parameters are assigned as $l_1 = 0.3$ m, $l_2 = 0.3$ m, $l_3 = 0.405$ m, $l_4 = 0.3$ m, $l_5 = 0.18$ m, $l_6 = 0.12$ m, and $l_7 = 0.12$ m. The radius of wheel is $R = 0.12$, and the radius of small wheel is $r = 0.05$ m. The step parameters are $h = 0.17$ m and $d = 0.25$ m. Moreover, $\delta = 0.66$ rad, $m_1 = 5$ kg, $m_2 = 4$ kg, $m_3 = 3$ kg, $m_4 = 3$ kg, $m_5 = 6$ kg, $m_6 = 3$ kg, and $m_7 = 3$ kg, and $j_1 = 0.6\,\text{kg}\cdot\text{m}^2$, $j_2 = 0.7\,\text{kg}\cdot\text{m}^2$, $j_3 = 0.03\,\text{kg}\cdot\text{m}^2$, $j_4 = 0.03\,\text{kg}\cdot\text{m}^2$, $j_5 = 0.04\,\text{kg}\cdot\text{m}^2$, $j_6 = 0.03\,\text{kg}\cdot\text{m}^2$, and $j_7 = 0.03\,\text{kg}\cdot\text{m}^2$. The rotational speed of climbing mechanisms $v = 1.675$ rad/s. The dynamics of the wheelchair is obtained in Section 2 by using these parameters. Choosing the process of the wheelchair climbing two steps, the desired position trajectories are designed according to analyzing the kinematic model in Section 2.

In this section, the position responses and tracking errors of Joint 1 and Joint 2 achieved by the two controllers are shown and compared. For comparison purpose, the simulation is implemented under the same condition by using the HOSM controller and the HOSM synchronous controller, respectively. The parameters of the two controllers are $c_0 = 61$, $c_1 = 70$, $k_1 = 80$, $k_2 = 120$, $k_3 = 100$, and $k_4 = 120$. They are properly chosen to assure that the system can get similar performance using different controllers, and they keep constant during the whole simulation.

First is the moment of inertia uncertainties simulation. The inertia of Joint 1 keeps constant during the whole simulation. The inertia of Joint 2 has been changed at 4 s, 8 s, and 12 s. The value of the step amplitude is $0.7\,\text{kg}\cdot\text{m}^2$; that means the inertia of Joint 2 increases or decreases by 100% every time.

Figures 8(a) and 8(c) show the position responses achieved by HOSM controller. The results of HOSM synchronous controller are shown in Figures 8(b) and 8(d). It can be seen that the position responses of the two joints are always tracking the desired trajectories effectively by using the two control schemes. There is no obvious overshoot at the startup stage, and the tracking curves of the synchronous controller are smoother at the startup stage.

Table 1: Simulation results in case 1.

Item	HOSMC maximum value (rad)	HOSM synchronous controller maximum value (rad)
Position error of Joint 1	2×10^{-4}	1.4×10^{-4}
Position error of Joint 2	4×10^{-4}	2.2×10^{-4}
Synchronization error	8.1×10^{-4}	3.75×10^{-4}

The tracking errors and synchronization errors are shown in Figure 9. When the inertia of Joint 2 changes abruptly, the maximum position error of Joint 1 reaches 2×10^{-4} rad (Figure 9(a)) using the HOSMC strategy, and the maximum position error of Joint 2 reaches 4×10^{-4} rad (Figure 9(c)) at the same time. When the HOSM synchronous controller is applied, the maximum position errors of the two joints are 1.4×10^{-4} rad (Figure 9(b)) and 2.2×10^{-4} rad (Figure 9(d)), respectively.

The simulation results are listed in Table 1. From the comparison of the data above, the system's tracking errors and synchronous error are reduced over 30% and 50%, respectively, by adopting the HOSM synchronous scheme. It is clear that the proposed scheme has a better control performance with respect to inertia uncertainties.

Then, the torque disturbance simulation is carried out. The system has torque disturbance and parameter uncertainties in this case. Torque disturbance is a square wave with a period of 10 s, and the amplitude is 50 N·m.

The parameters of the two controllers are the same as case 1. Figures 10(a)–10(d) show the position responses of the two joints. It can be found in Figure 11 that both controllers give response to the disturbance and uncertainties, but the proposed controller gives smaller error curves. After the disturbance is added, the maximum error of Joint 1

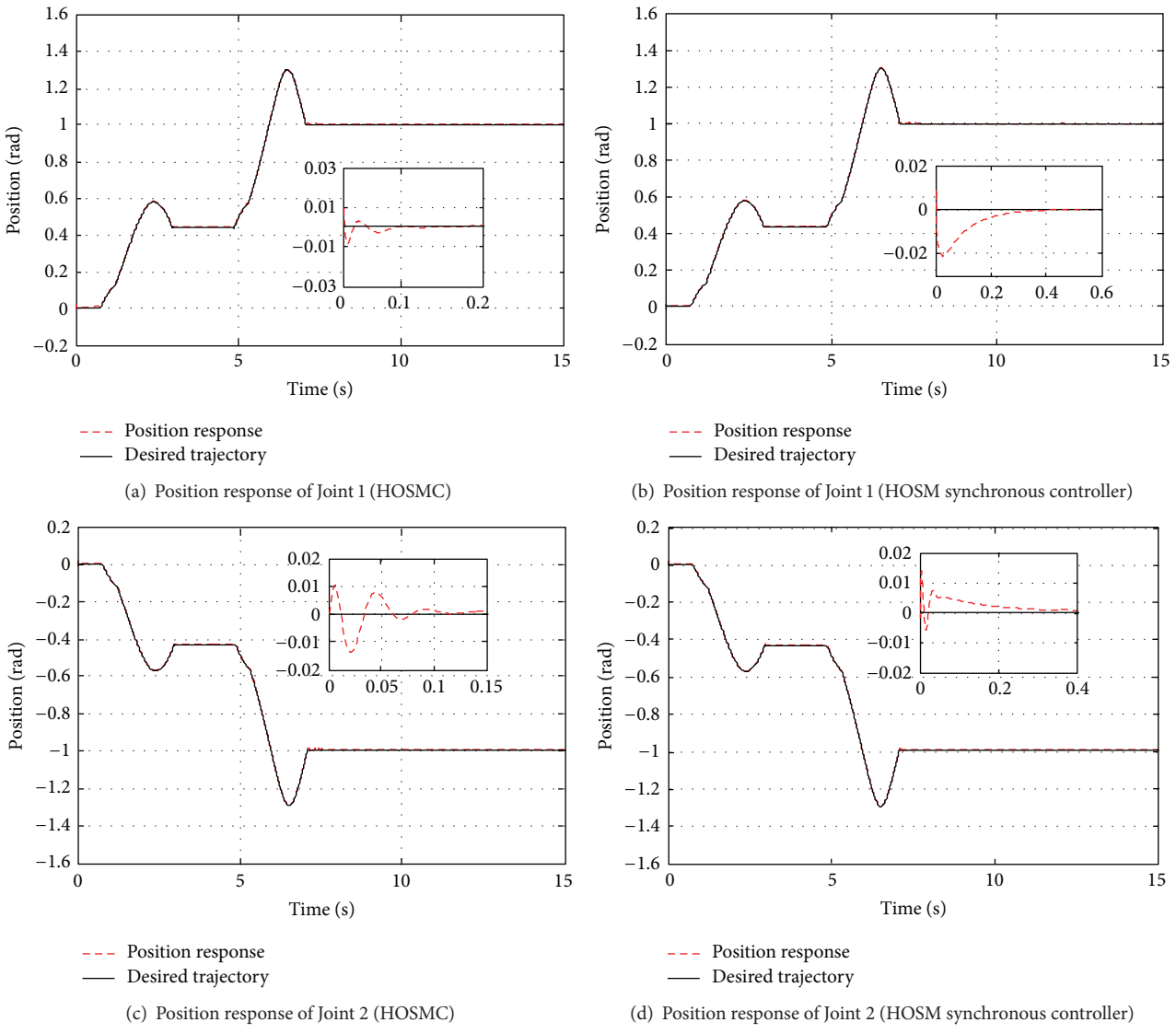

(a) Position response of Joint 1 (HOSMC)

(b) Position response of Joint 1 (HOSM synchronous controller)

(c) Position response of Joint 2 (HOSMC)

(d) Position response of Joint 2 (HOSM synchronous controller)

Figure 8: Position responses under inertia uncertainties.

Table 2: Simulation results in case 2.

Item	HOSMC maximum value (rad)	HOSM synchronous controller maximum value (rad)
Position error of Joint 1	3.1×10^{-4}	2×10^{-4}
Position error of Joint 2	4×10^{-4}	2.1×10^{-4}
Synchronization error	9.5×10^{-4}	5.5×10^{-4}

reaches 3.1×10^{-4} rad (Figure 11(a)) using the HOSMC strategy, and the maximum error of Joint 2 reaches 4×10^{-4} rad (Figure 11(c)) at the same time. When the HOSM synchronous controller is applied, the maximum errors of the two joints are 2×10^{-4} rad (Figure 11(b)) and 2.1×10^{-4} rad (Figure 11(d)), respectively. Figures 11(e) and 11(f) show the synchronization error curves.

The simulation results in case 2 are listed in Table 2. From the comparison of the data above, the system's position errors and synchronous error are reduced over 36% and 40% by adopting the HOSM synchronous scheme. It is clear that the HOSM synchronous controller has stronger robustness and higher performance. It also validates the correctness of the proposed scheme in this paper.

5. Conclusions

Considering a novel stair-climbing wheelchair with inertia uncertainties and torque disturbances, a HOSM controller is established, and closed-loop stability of the system is proved. Considering the synchronization of the system, a synchronous controller which combines

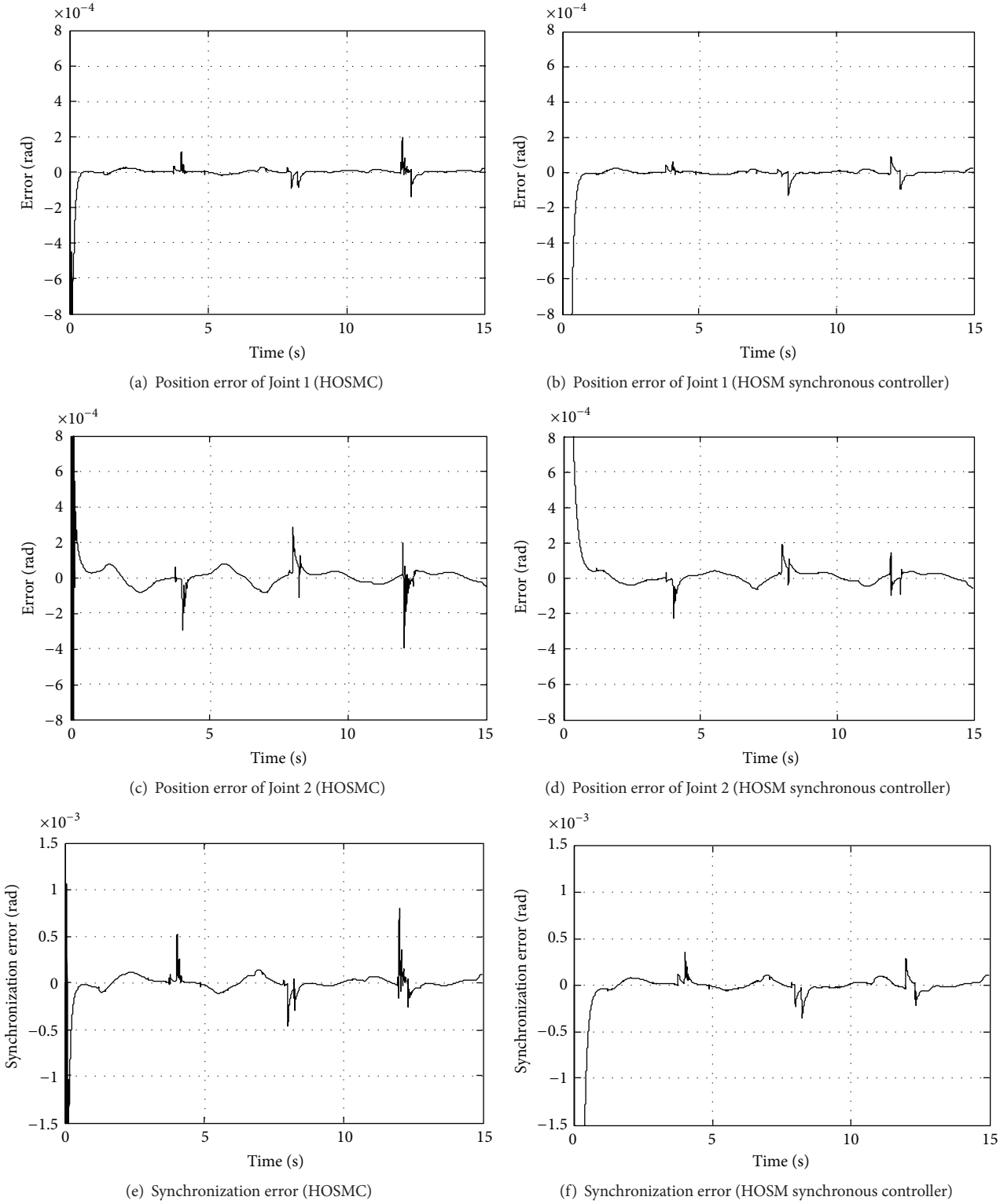

(a) Position error of Joint 1 (HOSMC)

(b) Position error of Joint 1 (HOSM synchronous controller)

(c) Position error of Joint 2 (HOSMC)

(d) Position error of Joint 2 (HOSM synchronous controller)

(e) Synchronization error (HOSMC)

(f) Synchronization error (HOSM synchronous controller)

Figure 9: Simulation results with inertia uncertainties.

the HOSMC techniques and cross-coupling techniques is proposed, and closed-loop stability of the system is proved, too. The simulation is performed in MATLAB to demonstrate the effectiveness of the proposed controller. The simulation results show that the proposed scheme can give better tracking performance with inertia uncertainties and torque disturbance and better synchronization.

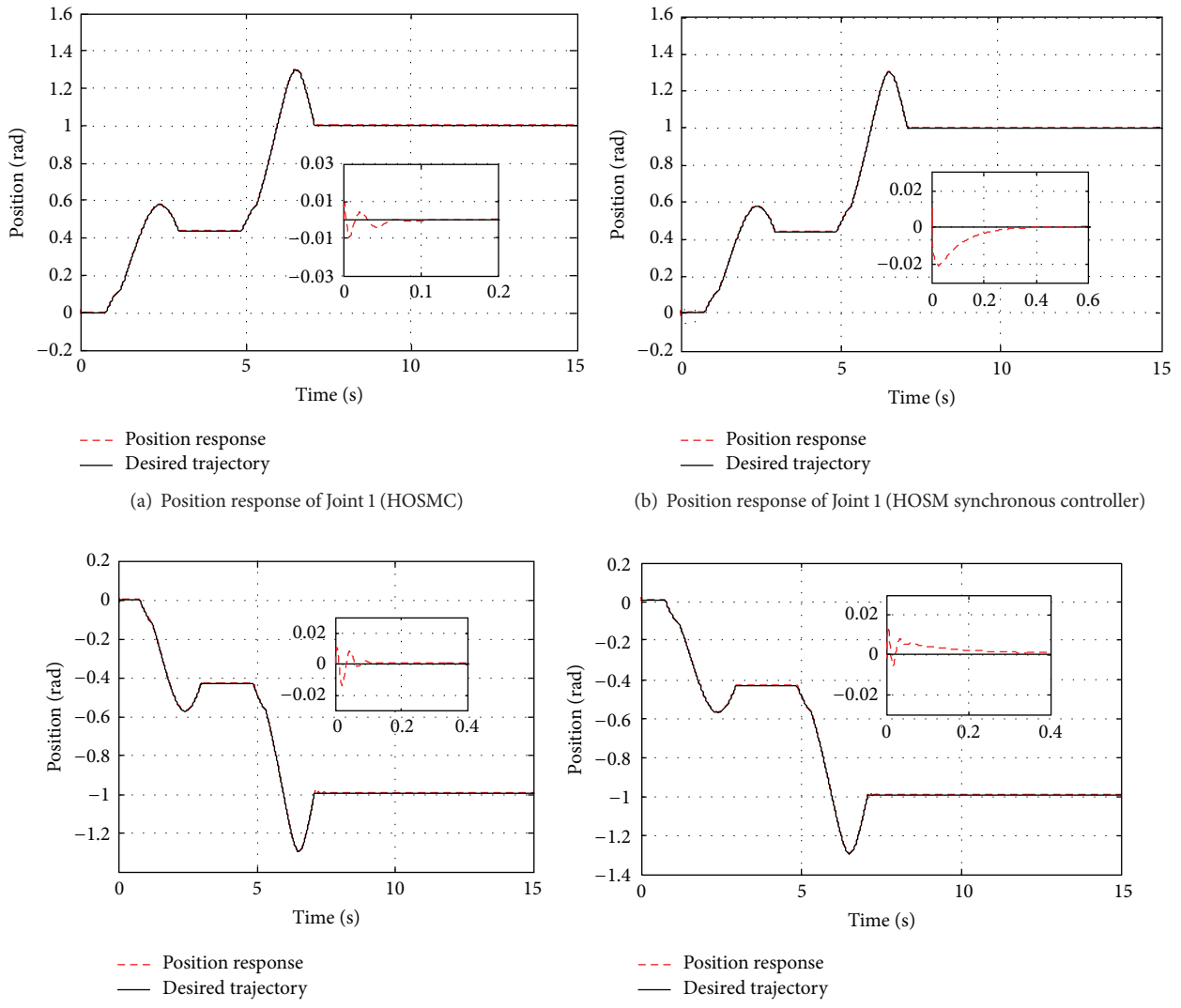

(a) Position response of Joint 1 (HOSMC)

(b) Position response of Joint 1 (HOSM synchronous controller)

(c) Position response of Joint 2 (HOSMC)

(d) Position response of Joint 2 (HOSM synchronous controller)

Figure 10: Position responses under inertia uncertainties and torque disturbance.

Appendix

The dynamic model in detail is

$$\begin{bmatrix} M_{11} & M_{12} & \cdots & M_{18} \\ M_{21} & M_{22} & & \\ \vdots & & \ddots & \vdots \\ M_{81} & & \cdots & M_{88} \end{bmatrix} \begin{bmatrix} \ddot{q}_0 \\ \ddot{q}_1 \\ \vdots \\ \ddot{q}_7 \end{bmatrix} + \begin{bmatrix} C_{11} & C_{12} & \cdots & C_{18} \\ C_{21} & C_{22} & & \\ \vdots & & \ddots & \vdots \\ C_{81} & & \cdots & C_{88} \end{bmatrix} \begin{bmatrix} \dot{q}_0 \\ \dot{q}_1 \\ \vdots \\ \dot{q}_7 \end{bmatrix} + \begin{bmatrix} G_1 \\ G_2 \\ \vdots \\ G_8 \end{bmatrix} g = \begin{bmatrix} \tau_0 \\ \tau_1 \\ \vdots \\ \tau_n \end{bmatrix}, \tag{A.1}$$

where g is the gravitational acceleration. M_{ij}, C_{ij}, and G_i are as follows:

$$M_{11} = j_0 + j_1 + j_2 + j_3 + j_4 + j_5 + j_6 + j_7 + (m_3 + m_4 + m_6 + m_7)(l_6 + r)^2 + (m_5 + m_6 + m_7) l_2^2 + (m_1 + m_2 + m_3 + m_4) l_3^2 + (m_2 + m_3 + m_4$$

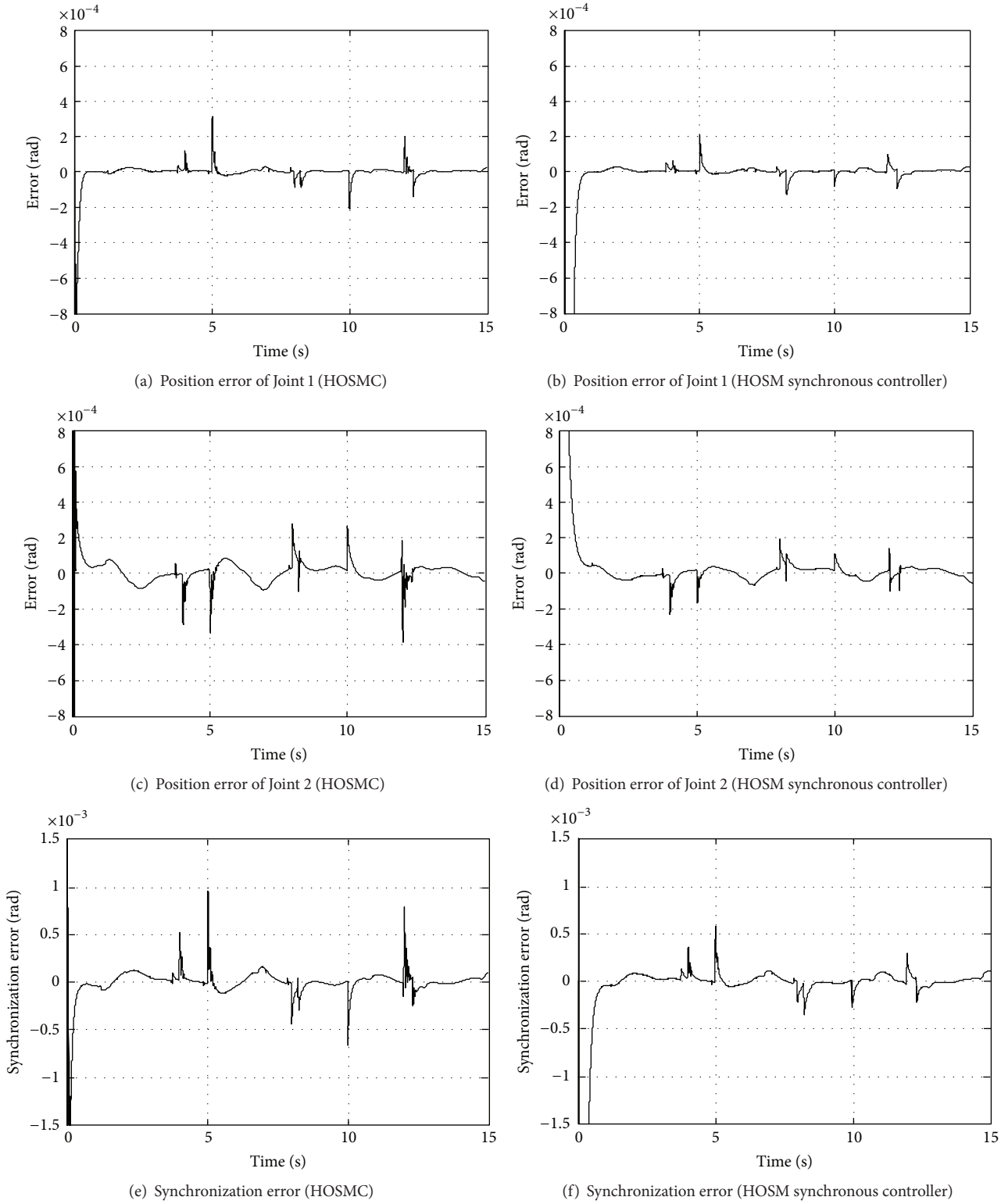

(a) Position error of Joint 1 (HOSMC)

(b) Position error of Joint 1 (HOSM synchronous controller)

(c) Position error of Joint 2 (HOSMC)

(d) Position error of Joint 2 (HOSM synchronous controller)

(e) Synchronization error (HOSMC)

(f) Synchronization error (HOSM synchronous controller)

Figure 11: Simulation results with inertia uncertainties and torque disturbance.

$$+ m_5 + m_6 + m_7) l_4^2 + (m_3 + m_4 + m_6 + m_7) l_5^2 + (m_2 + m_3 + m_4) l_3^2 \cos(q_2) - (m_3 - m_4) l_3 l_5 (1 + \cos(q_2)) - (m_3 \cos(q_3) - m_4 \cos(q_4)) l_3 (l_6 + r) - (m_3 \sin(q_3) - m_4 \sin(q_4)) l_4 (l_6 + r) + (m_3 \cos(q_3) + m_4 \cos(q_4)) l_5 (l_6 + r) - (m_2 + m_3 + m_4) l_3 l_4 \sin(q_2) - (m_3 \cos(q_3 - q_1) - m_4$$

$$\cdot \cos(q_4 - q_1)) l_3 (l_6 + r) + (m_6 \cos(q_6 - q_1) - m_7 \cos(q_7 - q_1)) l_2 (l_6 + r) + (m_6 \cos(q_6 - q_5) + m_7 \cos(q_7 - q_5)) l_5 (l_6 + r) - (m_6 \sin(q_6 - q_1) - m_7 \sin(q_7 - q_1)) l_4 (l_6 + r) + (m_6 - m_7) \cdot (\cos(q_1 - q_5) l_2 - \sin(q_5 - q_1) l_4) l_5,$$

$$M_{12} = j_1 + j_2 + j_3 + j_4 + m_3 (l_6 + r)^2 + (m_1 + m_2 + m_3 + m_4) l_3{}^2 + (m_2 + m_3 + m_4) \left(l_4{}^2 + l_3{}^2 \cdot \cos(q_2) - l_3 l_4 \sin(q_2)\right) + (m_3 + m_4) l_5{}^2 - (m_3 - m_4) l_3 l_5 (1 + \cos(q_2)) - (m_3 \cos(q_3) - m_4 \cdot \cos(q_4)) l_3 (l_6 + r) + (m_3 \cos(q_3) + m_4 \cos(q_4)) \cdot l_5 (l_6 + r) - (m_3 \sin(q_3) - m_4 \sin(q_4)) l_4 (l_6 + r) - (m_3 \cos(q_1 - q_3) - m_4 \cos(q_1 - q_4)) l_3 (l_6 + r),$$

$$M_{13} = j_2 + j_3 + j_4 + (m_3 + m_4) (l_6 + r)^2 + (m_2 + m_3 + m_4) \left(l_4{}^2 - l_3 l_4 \sin(q_2)\right) + (m_3 + m_4) l_5{}^2 - (m_3 - m_4) l_3 l_5 (1 + \cos(q_2)) - (m_3 \cos(q_3) - m_4 \cos(q_4)) l_3 (l_6 + r) + (m_3 \cos(q_3) + m_4 \cdot \cos(q_4)) l_5 (l_6 + r) - (m_3 \sin(q_3) - m_4 \sin(q_4)) \cdot l_4 (l_6 + r) - (m_3 \cos(q_1 - q_3) - m_4 \cdot \cos(q_1 - q_4)) l_3 (l_6 + r),$$

$$M_{14} = j_3 + m_3 (l_6 + r)^2 - m_3 (\cos(q_3) (l_3 - l_5) + \sin(q_3) l_4 + \cos(q_1 - q_3) l_3) (l_6 + r),$$

$$M_{15} = j_4 + m_4 (l_6 + r)^2 + m_4 (\cos(q_4) (l_3 + l_5) + \sin(q_4) l_4 + \cos(q_1 - q_4) l_3) (l_6 + r),$$

$$M_{16} = j_5 + m_5 (\cos(q_1 - q_5) l_2 - \sin(q_5 - q_1) l_4) R,$$

$$M_{17} = j_6 + m_6 (l_6 + r)^2 + m_6 (\cos(q_1 - q_6) l_2 + \cos(q_5 - q_6) l_5 - \sin(q_6 - q_1) l_4) (l_6 + r),$$

$$M_{18} = j_7 + m_7 (l_6 + r)^2 - m_7 (\cos(q_1 - q_7) l_2 - \cos(q_5 - q_7) l_5 - \sin(q_7 - q_1) l_4) (l_6 + r);$$

$$M_{21} = M_{12},$$

$$M_{22} = j_1 + j_2 + j_3 + j_4 + m_3 (l_6 + r)^2 + (m_2 + m_3 + m_4) \left(l_3{}^2 + \cos(q_2) l_3{}^2 - \sin(q_2) l_3 l_4 + l_4{}^2\right) + (m_3 + m_4) \left(l_5{}^2 - l_3 l_5\right) - m_3 \cos(q_3) (l_3 - l_5) (l_6 + r) - m_3 \sin(q_3) l_4 (l_6 + r) - m_3 \cos(q_2) l_3 l_5 + m_4 \cos(q_2) l_3 l_5 - m_3 \cos(q_1 - q_3) l_3 (l_6 + r),$$

$$M_{23} = j_2 + j_3 + j_4 + m_3 (l_6 + r)^2 + (m_2 + m_3 + m_4) \cdot \left(l_4{}^2 - l_3 l_4 \sin(q_2)\right) + (m_3 + m_4) l_5{}^2 - (m_3 - m_4) l_3 l_5 (1 + \cos(q_2)) - (m_3 \cos(q_3) - m_4 \cdot \cos(q_4)) l_3 (l_6 + r) + (m_3 \cos(q_3) + m_4 \cos(q_4)) \cdot l_5 (l_6 + r) - (m_3 \sin(q_3) - m_4 \sin(q_4)) l_4 (l_6 + r) - (m_3 \cos(q_1 - q_3) - m_4 \cos(q_1 - q_4)) l_3 (l_6 + r),$$

$$M_{24} = j_3 + m_3 (l_6 + r)^2 - m_3 ((l_3 - l_5) \cos(q_3) + l_4 \cdot \sin(q_3) + l_3 \cos(q_1 - q_3)) (l_6 + r),$$

$$M_{25} = j_4 + m_4 ((l_3 + l_5) \cos(q_4) + l_4 \sin(q_4) + l_3 \cdot \cos(q_1 - q_4)) (l_6 + r),$$

$$M_{26} = M_{27} = M_{28} = 0;$$

$$M_{31} = M_{13},$$

$$M_{32} = M_{23},$$

$$M_{33} = j_2 + j_3 + j_4 + (m_3 + m_4) (l_6 + r)^2 + (m_2 + m_3 + m_4) \left(l_4{}^2\right) + (m_3 + m_4) l_5{}^2 + (m_3 \cos(q_3) + m_4 \cos(q_4)) l_5 (l_6 + r) - (m_3 \sin(q_3) - m_4 \cdot \sin(q_4)) l_4 (l_6 + r),$$

$$M_{34} = j_3 + m_3 (l_6 + r)^2 + m_3 (\cos(q_3) l_5 - \sin(q_3) \cdot l_4) (l_6 + r),$$

$$M_{35} = j_4 + m_4 (l_6 + r)^2 + m_4 (\cos(q_4) l_5 + \sin(q_4) \cdot l_4) (l_6 + r),$$

$$M_{36} = M_{37} = M_{38} = 0;$$

$$M_{41} = M_{14},$$

$$M_{42} = M_{24},$$

$$M_{43} = M_{34},$$

$$M_{44} = j_3 + m_3 (l_6 + r)^2,$$

$$M_{45} = M_{46} = M_{47} = M_{48} = 0;$$

$$M_{51} = M_{15},$$

$$M_{52} = M_{25},$$

$$M_{53} = M_{35},$$

$$M_{54} = 0,$$

$$M_{55} = j_4 + m_4 (l_6 + r)^2,$$

$$M_{56} = M_{57} = M_{58} = 0;$$

$$M_{61} = M_{16},$$

$$M_{62} = M_{63} = M_{64} = M_{65} = 0,$$

$$M_{66} = j_5 + m_5 R^2,$$

$$M_{67} = M_{68} = 0;$$

$$M_{71} = M_{17},$$

$$M_{72} = M_{73} = M_{74} = M_{75} = M_{76} = 0,$$

$$M_{77} = j_6 + m_6 (l_6 + r)^2,$$

$$M_{78} = 0;$$

$$M_{81} = M_{18},$$

$$M_{82} = M_{83} = M_{84} = M_{85} = M_{86} = M_{87} = 0,$$

$$M_{88} = j_7 + m_7 (l_6 + r)^2,$$

$$C_{11} = ((m_2 l_3 + m_3 (l_3 - l_5) + m_4 (l_3 + l_5)) l_3 \sin(q_1) - m_5 (\sin(q_5 - q_1) l_2 + \cos(q_5 - q_1) l_4) R - m_7 \cdot \sin(q_7 - q_1) l_2 (l_6 + r)) \dot{q}_0,$$

$$C_{12} = \left((m_2 + m_3 + m_4) {l_3}^2 - (m_3 - m_4) l_3 l_5\right) \sin(q_1) \cdot (\dot{q}_1 + \dot{q}_0),$$

$$C_{13} = -(m_2 + m_3 + m_4) {l_3}^2 \dot{q}_2 - ((m_2 + m_3 + m_4) l_4 \cdot \cos(q_2) + (m_3 - m_4) l_5 \sin(q_1)) l_3 (\dot{q}_0 + \dot{q}_1 + \dot{q}_2) - (m_2 + m_3 + m_4) l_3 l_4 (\dot{q}_0 + \dot{q}_1) + (m_3 \cdot \sin(q_3) + m_3 \sin(q_3 - q_1) - m_4 \sin(q_4) - m_4 \cdot \sin(q_4 - q_1)) l_3 (l_6 + r) (\dot{q}_0 + \dot{q}_1 + \dot{q}_2),$$

$$C_{14} = m_3 (l_3 \sin(q_3) - l_4 \cos(q_3) - l_5 \sin(q_3) + l_3 \cdot \sin(q_3 - q_1)) (l_6 + r) (\dot{q}_0 + \dot{q}_1 + \dot{q}_2 + \dot{q}_3),$$

$$C_{15} = m_4 (l_4 \cos(q_4) - l_5 \sin(q_4) - l_3 \sin(q_4) - l_3 \cdot \sin(q_4 - q_1)) (l_6 + r) (\dot{q}_0 + \dot{q}_1 + \dot{q}_2 + \dot{q}_4),$$

$$C_{16} = -m_5 l_2 R \sin(q_5 - q_1) (\dot{q}_0 + \dot{q}_5) - m_5 l_4 R \cos(q_5 - q_1) (\dot{q}_0 + \dot{q}_5),$$

$$C_{17} = -m_6 (l_4 \cos(q_6 - q_1) + l_5 \sin(q_6 - q_5) + l_2 \cdot \sin(q_6 - q_1)) (l_6 + r) (\dot{q}_0 + \dot{q}_6),$$

$$C_{18} = m_7 (l_4 \cos(q_7 - q_1) - l_5 \sin(q_7 - q_5) - l_2 \cdot \sin(q_7 - q_1)) (l_6 + r) (\dot{q}_0 + \dot{q}_7);$$

$$C_{21} = ((m_2 l_3 + m_3 (l_3 - l_5) + m_4 (l_3 + l_5)) l_3 \sin(q_1) + m_4 (l_4 \cos(q_4) - (l_3 + l_5) \sin(q_4) - l_3 \sin(q_4 - q_1)) (l_6 + r)) \dot{q}_0,$$

$$C_{22} = (((m_2 + m_3 + m_4) l_3 - m_3 l_5 + m_4 l_5) l_3 \sin(q_1) + m_4 (l_4 \cos(q_4) - (l_3 + l_5) \sin(q_4) - l_3 \sin(q_4 - q_1)) (l_6 + r)) (\dot{q}_0 + \dot{q}_1),$$

$$C_{23} = -((m_2 + m_3 + m_4) l_3 l_4 (1 + \cos(q_2)) + (m_3 - m_4) l_3 l_5 \sin(q_1) - (m_3 l_3 (\sin(q_3) + \sin(q_3 - q_1)) - m_4 (l_3 + l_5) \sin(q_4) + m_4 l_4 \cos(q_4) - m_4 l_3 \sin(q_4 - q_1)) (l_6 + r)) (\dot{q}_0 + \dot{q}_1 + \dot{q}_2),$$

$$C_{24} = m_3 (l_3 \sin(q_3) - l_4 \cos(q_3) - l_5 \sin(q_3) + l_3 \cdot \sin(q_3 - q_1)) (l_6 + r) (\dot{q}_0 + \dot{q}_1 + \dot{q}_2 + \dot{q}_3),$$

$$C_{25} = m_4 (l_4 \cos(q_4) - l_5 \sin(q_4) - l_3 \sin(q_4) - l_3 \cdot \sin(q_4 - q_1)) (l_6 + r) (\dot{q}_0 + \dot{q}_1 + \dot{q}_2 + \dot{q}_4),$$

$$C_{26} = C_{27} = C_{28} = 0;$$

$$C_{31} = (m_2 + m_3 + m_4) l_3 l_4 (1 + \cos(q_2)) \dot{q}_0 - (m_3 \cdot \sin(q_3) + m_4 \sin(q_4) + m_3 \sin(q_3 - q_1) - m_4 \cdot \sin(q_4 - q_1)) l_3 (l_6 + r) \dot{q}_0,$$

$$C_{32} = (m_2 + m_3 + m_4) l_3 l_4 (1 + \cos(q_2)) (\dot{q}_0 + \dot{q}_1) - (m_3 \sin(q_3) - m_4 \sin(q_4) + m_3 \sin(q_3 - q_1) - m_4 \sin(q_4 - q_1)) l_3 (l_6 + r) (\dot{q}_0 + \dot{q}_1),$$

$$C_{33} = 0,$$

$$C_{34} = -m_3 (l_4 \cos(q_3) + l_5 \sin(q_3)) (l_6 + r) (\dot{q}_0 + \dot{q}_1 + \dot{q}_2 + \dot{q}_3),$$

$$C_{35} = m_4 (l_4 \cos(q_4) - l_5 \sin(q_4)) (l_6 + r) (\dot{q}_0 + \dot{q}_1 + \dot{q}_2 + \dot{q}_3),$$

$$C_{36} = C_{37} = C_{38} = 0;$$

$$C_{41} = m_3 (l_4 \cos(q_3) - (l_3 - l_5) \sin(q_3) - l_3 \cdot \sin(q_3 - q_1)) (l_6 + r) \dot{q}_0,$$

$$C_{42} = m_3 (l_4 \cos(q_3) - (l_3 - l_5) \sin(q_3) - l_3 \cdot \sin(q_3 - q_1)) (l_6 + r) (\dot{q}_0 + \dot{q}_1),$$

$$
\begin{aligned}
C_{43} &= m_3\left(l_4\cos\left(q_3\right)+l_5\sin\left(q_3\right)\right)\left(l_6+r\right)\left(\dot{q}_0+\dot{q}_1\right.\\
&\quad\left.+\dot{q}_2\right),\\
C_{44} &= C_{45}=C_{46}=C_{47}=C_{48}=0;\\
C_{51} &= m_4\left(\left(l_3+l_5\right)\sin\left(q_4\right)-l_4\cos\left(q_4\right)+l_3\right.\\
&\quad\left.\cdot\sin\left(q_4-q_1\right)\right)\left(l_6+r\right)\dot{q}_0,\\
C_{52} &= m_4\left(\left(l_3+l_5\right)\sin\left(q_4\right)-l_4\cos\left(q_4\right)+l_3\right.\\
&\quad\left.\cdot\sin\left(q_4-q_1\right)\right)\left(l_6+r\right)\left(\dot{q}_0+\dot{q}_1\right),\\
C_{53} &= m_4\left(l_5\sin\left(q_4\right)-l_4\cos\left(q_4\right)\right)\left(l_6+r\right)\left(\dot{q}_0+\dot{q}_1\right.\\
&\quad\left.+\dot{q}_2\right),\\
C_{54} &= C_{55}=C_{56}=C_{57}=C_{58}=0;\\
C_{61} &= m_5\left(l_2\sin\left(q_5-q_1\right)+l_4\cos\left(q_5-q_1\right)\right)R\dot{q}_0,\\
C_{62} &= C_{63}=C_{64}=C_{65}=C_{66}=C_{67}=C_{68}=0;\\
C_{71} &= m_6\left(l_2\sin\left(q_6-q_1\right)+l_4\cos\left(q_6-q_1\right)+l_5\right.\\
&\quad\left.\cdot\sin\left(q_6-q_5\right)\right)\left(l_6+r\right)\dot{q}_0,\\
C_{72} &= C_{73}=C_{74}=C_{75}=C_{76}=C_{77}=C_{78}=0;\\
C_{81} &= m_7\left(-l_2\sin\left(q_7-q_1\right)-l_4\cos\left(q_7-q_1\right)+l_5\right.\\
&\quad\left.\cdot\sin\left(q_7-q_5\right)\right)\left(l_6+r\right)\dot{q}_0,\\
C_{82} &= C_{83}=C_{84}=C_{85}=C_{86}=C_{87}=C_{88}=0,\\
G_1 &= \left(m_2+m_3+m_4\right)l_3-\left(m_3-m_4\right)l_5+\left(m_1+m_2\right.\\
&\quad\left.+m_3+m_4\right)l_3\cos\left(q_1\right)-\left(m_5+m_6+m_7\right)\left(l_2\right.\\
&\quad\left.\cdot\cos\left(q_1\right)+l_4\sin\left(q_1\right)\right)-\left(m_6-m_7\right)l_5\cos\left(q_5\right)\\
&\quad-\left(m_3\cos\left(q_3\right)+m_6\cos\left(q_6\right)+m_4\sin\left(q_4\right)+m_7\right.\\
&\quad\left.\cdot\sin\left(q_7\right)\right)\left(l_6+r\right),\\
G_2 &= \left(m_2+m_3+m_4\right)l_3-\left(m_3-m_4\right)l_5+\left(m_1+m_2\right.\\
&\quad\left.+m_3+m_4\right)l_3\cos\left(q_1\right)-m_3\left(l_6+r\right)\cos\left(q_3\right),\\
G_3 &= -\left(m_3-m_4\right)l_5-\left(m_3\cos\left(q_3\right)+m_4\sin\left(q_4\right)\right)\\
&\quad\cdot\left(l_6+r\right),\\
G_4 &= -m_3\cos\left(q_3\right)\left(l_6+r\right),\\
G_5 &= -m_4\sin\left(q_4\right)\left(l_6+r\right),\\
G_6 &= -m_5\cos\left(q_5\right)R,\\
G_7 &= -m_6\cos\left(q_6\right)\left(l_6+r\right),\\
G_8 &= -m_7\sin\left(q_7\right)\left(l_6+r\right).
\end{aligned}
\tag{A.2}
$$

Conflict of Interests

The authors declare that there is no conflict of interests regarding the publication of this paper.

Acknowledgment

This work was supported by the National Natural Science Foundation of China under Grant no. 61074023.

References

[1] M. J. Lawn, T. Sakai, M. Kuroiwa, and T. Ishimatsu, "Development and practical application of a stairclimbing wheelchair in Nagasaki," *Journal of HWRS-ERC*, vol. 2, no. 2, pp. 33–39, 2001.

[2] N. M. A. Ghani, M. O. Tokhi, A. N. K. Nasir, and S. Ahmad, "Control of a stair climbing wheelchair," *IAES International Journal of Robotics and Automation*, vol. 1, no. 4, pp. 203–213, 2012.

[3] G. Quaglia, W. Franco, and R. Oderio, "Wheelchair.q, a mechanical concept for a stair climbing wheelchair," in *Proceedings of the IEEE International Conference on Robotics and Biomimetics (ROBIO '09)*, pp. 800–805, IEEE, Guilin, China, December 2009.

[4] T. Mabuchi, T. Nagasawa, K. Awa, K. Shiraki, and T. Yamada, "Development of a stair-climbing mobile robot with legs and wheels," *Artificial Life and Robotics*, vol. 2, no. 4, pp. 184–188, 1998.

[5] C.-T. Chen and H.-V. Pham, "Design and fabrication of a statically stable stair-climbing robotic wheelchair," *Industrial Robot*, vol. 36, no. 6, pp. 562–569, 2009.

[6] M. J. Lawn and T. Ishimatsu, "Modeling of a stair-climbing wheelchair mechanism with high single-step capability," *IEEE Transactions on Neural Systems and Rehabilitation Engineering*, vol. 11, no. 3, pp. 323–332, 2003.

[7] Y. Sugahara, N. Yonezawa, and K. Kosuge, "A novel stair-climbing wheelchair with transformable wheeled four-bar linkages," in *Proceedings of the 23rd IEEE/RSJ International Conference on Intelligent Robots and Systems (IROS '10)*, pp. 3333–3339, IEEE, Taipei, Taiwan, October 2010.

[8] D. Davies and S. Hirose, "Continuous high-speed climbing control and leg mechanism for an eight-legged stair-climbing vehicle," in *Proceedings of the IEEE/ASME International Conference on Advanced Intelligent Mechatronics (AIM '09)*, pp. 1606–1612, IEEE, Singapore, July 2009.

[9] E. Mihankhah, A. Kalantari, E. Aboosaeedan, H. D. Taghirad, and S. A. A. Moosavian, "Autonomous staircase detection and stair climbing for a tracked mobile robot using fuzzy controller," in *Proceedings of the IEEE International Conference on Robotics and Biomimetics (ROBIO '08)*, pp. 1980–1985, IEEE, Bangkok, Thailand, February 2009.

[10] J. Wang, T. Wang, C. Yao, X. Li, and C. Wu, "Dynamic modeling and control for WT wheelchair robot during the stair-climbing process," *Journal of Mechanical Engineering*, vol. 50, no. 13, pp. 22–34, 2014.

[11] H. Lee and V. I. Utkin, "Chattering suppression methods in sliding mode control systems," *Annual Reviews in Control*, vol. 31, no. 2, pp. 179–188, 2007.

[12] G. Bartolini, A. Ferrara, and E. Usai, "Chattering avoidance by second-order sliding mode control," *IEEE Transactions on Automatic Control*, vol. 43, no. 2, pp. 241–246, 1998.

[13] K.-M. Ma, "Design of higher order sliding mode attitude control laws for large-scale spacecraft," *Control and Decision*, vol. 28, no. 2, pp. 201–210, 2013.

[14] A. Arisoy, M. K. Bayrakceken, S. Basturk, M. Gokasan, and O. S. Bogosyan, "High order sliding mode control of a space robot manipulator," in *Proceedings of the 5th International Conference on Recent Advances in Space Technologies (RAST '11)*, pp. 833–838, IEEE, Istanbul, Turkey, June 2011.

[15] D. Sun, X. Shao, and G. Feng, "A model-free cross-coupled control for position synchronization of multi-axis motions: theory and experiments," *IEEE Transactions on Control Systems Technology*, vol. 15, no. 2, pp. 306–314, 2007.

[16] D. Zhao, S. Li, F. Gao, and Q. Zhu, "Robust adaptive terminal sliding mode-based synchronised position control for multiple motion axes systems," *IET Control Theory & Applications*, vol. 3, no. 1, pp. 136–150, 2009.

[17] F.-J. Lin, P.-H. Chou, C.-S. Chen, and Y.-S. Lin, "DSP-based cross-coupled synchronous control for dual linear motors via intelligent complementary sliding mode control," *IEEE Transactions on Industrial Electronics*, vol. 59, no. 2, pp. 1061–1073, 2012.

[18] J. X. Liu and Q. W. Chen, "Dynamics and control study of a stair-climbing walking aid robot," in *Proceedings of the International Conference on Mechanic Automation and Control Engineering (MACE '10)*, pp. 6190–6194, IEEE, Wuhan, China, June 2010.

[19] R. Morales, A. Gonzalez, V. Feliu, and P. Pintado, "Environment adaptation of a new staircase-climbing wheelchair," *Autonomous Robots*, vol. 23, no. 4, pp. 275–292, 2007.

[20] J. X. Liu, Y. F. Wu, J. Guo, R. Li, and Q. W. Chen, "Modeling and simulation analysis of a walking assistant robot for both plane and stair," *Chinese Journal of Engineering Design*, vol. 22, no. 4, pp. 344–350, 2015.